Quantifying the Stable Boundary Layer Depth in the Arctic Region of Northern Finland

THERESA LINCHECK*

National Weather Center Research Experiences for Undergraduates Program
Norman, Oklahoma

BRIAN R. GREENE, FRANCESCA M. LAPPIN, AND ELIZABETH A. PILLAR-LITTLE
School of Meteorology, University of Oklahoma
Center for Autonomous Sensing and Sampling, University of Oklahoma
Norman, Oklahoma

ABSTRACT

The complex structure of the nighttime Arctic stable boundary layer (SBL) has long impeded the development of a comprehensive SBL depth parametrization, consequently leading to poor representation in many climate models. This study attempts to quantify the depth of the SBL in the Arctic region of Finland using high-resolution vertical profile data of temperatures, horizontal wind speeds, and directions extrapolated from in-situ rotary-wing unmanned aircraft systems (rwUAS) flown during the 2018 Innovative Strategies for Observations in the Arctic Atmospheric Boundary Layer (ISOBAR) field campaign. Two SBL depth parametrizations are investigated – 1) the height of the maximum potential temperature gradient and 2) the height of the maximum horizontal wind speed magnitude, or lowest low-level jet height. Initial attempts at calculating a single consistent maximum temperature gradient proved difficult, and averaging and filtering methods were employed to improve chances of observing reasonable heights. The addition of horizontal wind directions as wind vectors to temperature profiles helped offer insights into the behavior of the inversions and confirm or invalidate the maximum gradient heights. Investigating maximum wind speed heights revealed they consistently formed around 80 m-100 m above the maximum temperature gradient heights. Analyses of the three SBL profiles altogether - temperature, wind speed, and direction – propounded the possibility of their usage in creating a more explicit SBL depth parametrization. The results also demonstrated the capabilities of rwUAS as a promising tool for improving understandings of the SBL structure.

1. Introduction

Prolonged winter nights in the Arctic region, alongside ice-covered surfaces and moderately cool temperatures, often produce an ideal environment for the formation of a stable boundary layer (SBL). Within these SBLs, turbulence is weak and dominated by shear forces, airflow is locally quasi-laminar and stagnant, and radiative surface cooling is strong (Stull 1988; Mayfield and Fochesatto 2013). Also, as the Earth's surface cools faster than the air above, it creates a temperature inversion, or positive upward temperature gradient, which becomes characteristic of strong SBLs. Typical SBLs significantly influence near-surface as well as large-scale atmospheric dynamics (Huang and Bou-Zeid 2013; Curry 1983; Pithan et al. 2014). As such an in-depth understanding of the SBL structure is needed to improve parameterization in large-scale models for various aspects of numerical weather prediction (NWP) and climate modelling such as land surface temperature forecasting at night, fog prediction, timing of convection, and polar climate (Beare et al. 2006; Sandu et al. 2013; Newman and Klein 2014).

While a better understanding of the stable boundary layer is needed for accurate forecasts, difficulties and limitations in both field observations and numerical simulations (Huang and Bou-Zeid 2013; Steeneveld et al. 2008; Sandu et al. 2013) have made significant advancements challenging. Turbulent eddies in the SBL exist on much smaller scales than in the convective boundary layer (CBL), thus they require significantly higher resolution and computational power from Large Eddy Simulations (LES) to maintain resolved turbulence and provide a reliable simulation (Beare et al. 2006; Couvreux et al. 2020). Moreover, the small turbulent eddy sizes and weak fluxes often negatively affect the quality and representativity of field data (Huang and Bou-Zeid 2013). For example, temperature profiles retrieved from radiosondes often do not contain measurements with high enough vertical resolutions to pick up fluctuations caused by the weak turbulence. Instruments such as Doppler lidars can fill this

* *Corresponding author address:* Theresa Lincheck, Cleveland State University, 2121 Euclid Ave, Cleveland, OH 44115
E-mail: tlincheck@gmail.com

"planetary boundary layer (PBL) data gap" with higher resolution temperature and wind speed profiles, however high costs and sensitivity to environments of high reflectivity such as the Arctic remains a major impediment to their large-scale deployment in field studies (National Academies of Sciences 2018b,a; Hoff and Hardesty 2012; National Research Council 2007).

With the numerous observational and modelling hurdles present in studying the SBL structure, the development of unmanned aircraft systems (UAS) as weather-sensing and sampling tools offers a unique and unrivaled opportunity for improved observations of the SBL (Kral et al. 2018, 2020, in review) and a means to fill the PBL data gap. In particular, rotary wing multicopter unmanned aircraft systems (rwUAS) possess capabilities of retrieving very high vertical resolution profiles of temperature, humidity, pressure, and wind speeds starting at near-surface. Coupled with their relatively inexpensive, reusable, and adaptable design, rwUAS present new opportunities to better discover and understand the physical processes taking place within the stable boundary layer (Chilson et al. 2019).

Definitions and parametrizations of the stable boundary layer depth vary across literature and studies and include everything from maximum potential temperature gradients to minimum heights of low-level jets to the top of the stress layer (Stull 1988). However, many of these parameterizations fail to fully characterize the SBL depth, both due to the lack of SBL understanding and a shortage of high-resolution stable boundary layer measurements previously discussed. As UAS technology rapidly becomes commercialized and more readily accessible for researchers, it is now possible to use higher resolution UAS data to improve and even redefine known SBL depth parametrizations.

Accordingly, this project incorporates the use of rotary wing multicopter data as a principal means to learn more about the SBL structure in the Arctic region of northern Finland. This study attempts to use the multicopter temperature, wind speed, and direction profiles to quantify a reasonable SBL depth based on common existing SBL depth definitions. Finally, the scope of this project also extends to evaluating the potential of using multicopter observations for developing new and improved SBL depth parameterizations for future use in forecasts and climate models.

2. Data and Methods

a. ISOBAR 2018 Field Campaign

To investigate the structure of the SBL, this study uses observational data taken from the 2018 Innovative Strategies for Observations in the Arctic Atmospheric Boundary Layer (ISOBAR) field campaign which took place between February 6th - February 26th, 2018 on the island of Hailuoto, Finland. Field operations were primarily conducted on sea ice immediately west of the island at 65.037°N and 24.555°E during night-time hours and employed the use of instrumentation such as sonic anemometers and net radiation systems on meteorological towers, ground based sensors including Doppler lidar and sodar, and several rwUAS developed from University of Oklahoma Center for Autonomous Sensing and Sampling (OU-CASS) alongside German and Norwegian counterparts for collecting detailed observational measurements of the nighttime boundary layer (Kral et al. 2018, 2020, in review). Days during the ISOBAR field campaign had only around 7 to 10 hours of daylight, resulting in strong radiational surface cooling during most nights that created favorable conditions for consistent stable boundary layer formation. One of these days, February 18th, had exceptionally clear skies and strong radiational surface cooling resulting in a prolonged nighttime stable boundary layer, and is therefore used as a case study in this project.

For purposes of this study, data is primarily analyzed from the CopterSonde (Greene et al. 2018, 2019; Segales et al. 2020), a rotary wing UAS developed by OU-CASS and flown roughly every twenty minutes throughout several nights during the ISOBAR field campaign. During the ascent phase of the CopterSonde on these nights, including February 18th, high-resolution quasi-instantaneous profiles of temperature, relative humidity, pressure, horizontal wind speeds, and wind directions up to 300 m altitude were recorded. As discussed earlier, rwUAS technology such as the CopterSonde are capable of recording profiles on much higher spatial and temporal resolutions than traditional observational methods while still maintaining high levels of accuracy and precision (Bell et al. 2020; Barbieri et al. 2019), and is demonstrated in Fig. 1 below. Throughout the rest of this study, these high resolution rwUAS profiles will be the focus of all data analysis.

b. Calculating SBL Depth from CopterSonde data

In choosing the SBL depth parametrizations to be investigated using CopterSonde data, selections were made based on the following criteria – 1) it should be recurrent enough across literature and studies to be considered pertinent for future SBL study, 2) have potential for use and replication in climate models, and 3) practical to determine from the CopterSonde data alone. By using these three criteria, it could be ensured that any SBL depth parametrizations studied could be easily replicated using UAS but also have potential relevance for relating back to other instruments and models for future comparison studies. With this in mind, it was decided that two SBL depth parametrizations would be further explored in this study – the height z_i where the potential temperature gradient $\frac{\partial \theta}{\partial z}$ is maximum, and the height z_j where the horizontal wind speed magnitude $\left|\mathbf{U}\right|$ is maximum.

The first SBL depth investigated for the night of February 18th was the height z_i where the change in the potential

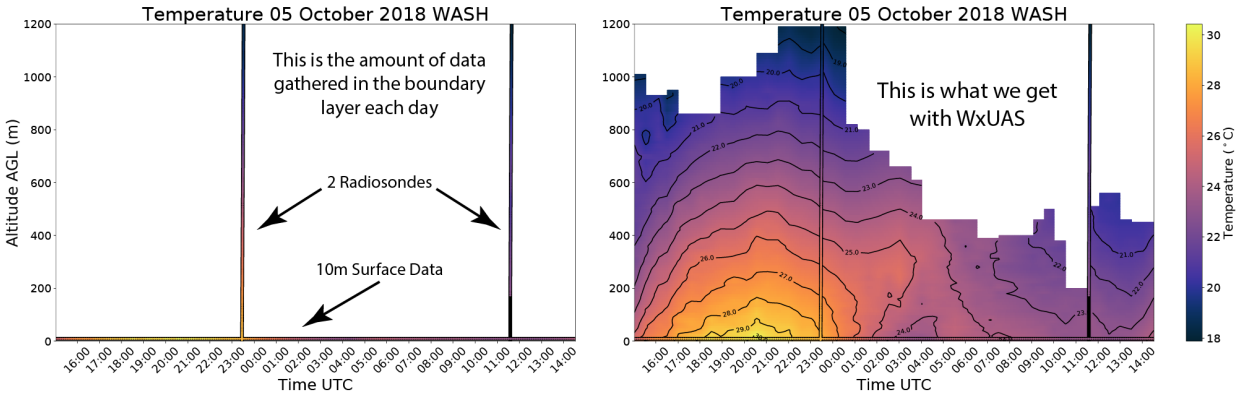

FIG. 1: Comparison between temperature observations collected from radiosonde soundings (left) versus CopterSonde temperature observations (right) during the 2018 Flux-Capacitor campaign in Washington, OK on October 5th. Figure from Bell (2019).

temperature $\frac{\partial\theta}{\partial z}$ was a maximum. In order to more easily find this maximum, CopterSonde temperature profiles were first smoothed using a low-pass filter with a cutoff frequency of 0.1 Hz and calibrated to one of the towers set up during the campaign. The output temperature profiles were then converted into potential temperature profiles using the equation

$$\theta = T \times \left(\frac{p_0}{p}\right)^{\frac{R_d}{c_p}} \tag{1}$$

where $p_0 = 1000$ hPa is standard pressure, $R_d = 287$ J kg^{-1}K^{-1} the dry air gas constant, and $c_p = 1004$ J kg^{-1}K^{-1} the specific heat constant. The ∂z differentials for $\frac{\partial\theta}{\partial z}$ were derived from altitude measurements recorded by the CopterSonde corresponding to the temperature measurements, and gradients were calculated using second-order finite differences except at the boundaries, where first-order differences were calculated instead. The very high spatial resolution (<1m) of the temperature measurements often resulted in height differentials ∂z becoming exceedingly small, especially within the initial 50 m of CopterSonde ascent. These small height differentials frequently caused "false" z_i heights to be located much lower than expected, usually within the first several meters from the surface. As an attempt to avoid calculating these false heights, the temperature data were regridded onto coarser height resolutions (Δz = 5 m, 10 m) by averaging all temperature data points in-between the new heights in a method similar to taking running linear averages. This regridding method worked to remove most, but not all, false z_i or low altitude locations where temperature gradients seemed maximum, as will be shown in the results below. To further remove the falsely reported z_i, filters were employed to ignore any maxima below 20 m and 50 m during analysis. This method also had variable success and will be further discussed in the results below.

Despite efforts to remove erroneous z_i heights with the methods discussed, uncertainty in the final z_i still remained. To mitigate this uncertainty, horizontal wind directions were compared above and below the z_i heights as a secondary means to support or contradict the validity of the z_i. This was done by first retrieving wind direction λ and wind speed $|\mathbf{U}|$ profiles from the CopterSonde. Conversions to the horizontal wind speed u and v components were then accomplished using the equations

$$u = -|\mathbf{U}| \times \sin\left(\lambda \times \frac{\pi}{180}\right) \tag{2}$$

$$v = -|\mathbf{U}| \times \cos\left(\lambda \times \frac{\pi}{180}\right) \tag{3}$$

Once the u,v wind profiles were found, they were used to generate and overlay corresponding wind vectors over the potential temperature plots and examine how the wind directions accentuated, or refuted, the validity of the z_i found from the maximum temperature gradients.

The second SBL depth examined using CopterSonde data was the height z_j where the wind speed magnitude $|\mathbf{U}|$ is maximum. Similar to the temperature data, the wind speed data was first processed to smooth the profile and calibrated against the Doppler lidar to help eliminate excess noise. After that, the height z_j of the maximum wind speed value was easily found and compared to the z_i heights previously found, as will be seen below in the results.

3. Results and Discussion

a. SBL depth determined by $\frac{\partial\theta}{\partial z}$ maxima

As briefly mentioned in the methods, the process for locating a singular height z_i proved difficult due to the high

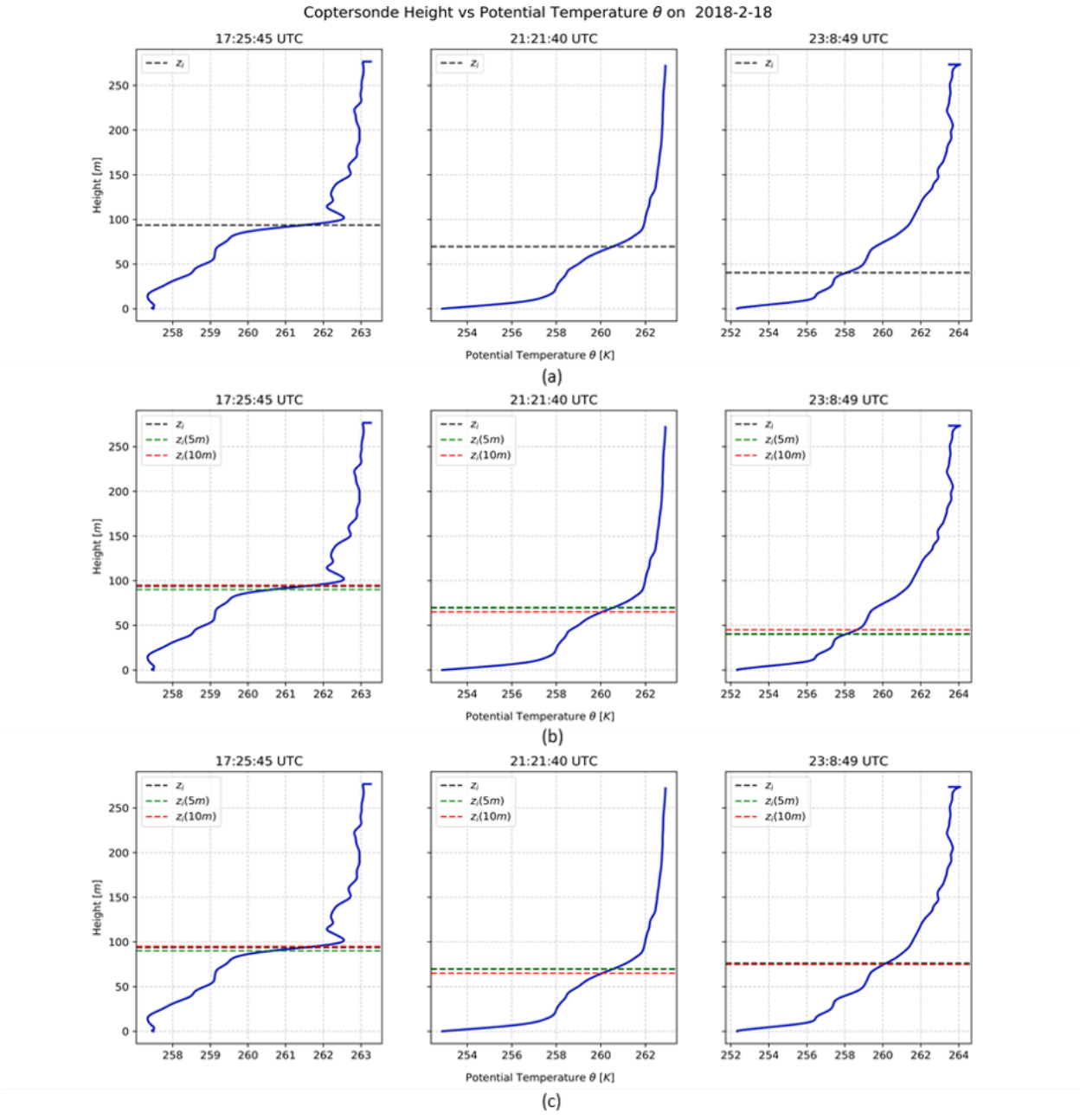

FIG. 2: CopterSonde potential temperature (K) profiles at three separate times during the night of February 18th. (a) Initial profiles are plotted along with the height z_i (black dotted line) where the maximum potential temperature gradients $\frac{\partial\theta}{\partial z}$ are calculated. (b) Initial z_i is compared to z_{i5m}, z_{i10m} with data regridded to coarser resolutions of 5 m and 10 m. (c) All z_i heights found <50m are filtered out. Notice rightmost plot therefore has a new z_i height around 75m.

resolution of the rwUAS temperature data and the theoretical nature of this z_i definition. Fig. 2 shows the potential temperature profiles examined at three different times during the night of February 18th, and compares the z_i heights calculated initially with heights calculated after regridding and filtering the data to remove "false" or unreasonably low z_i.

Fig. 2a exhibits the initial potential temperature profiles as well as the z_i heights where the gradient maximum, and hence the SBL depth, is observed. Notice in all three pro-

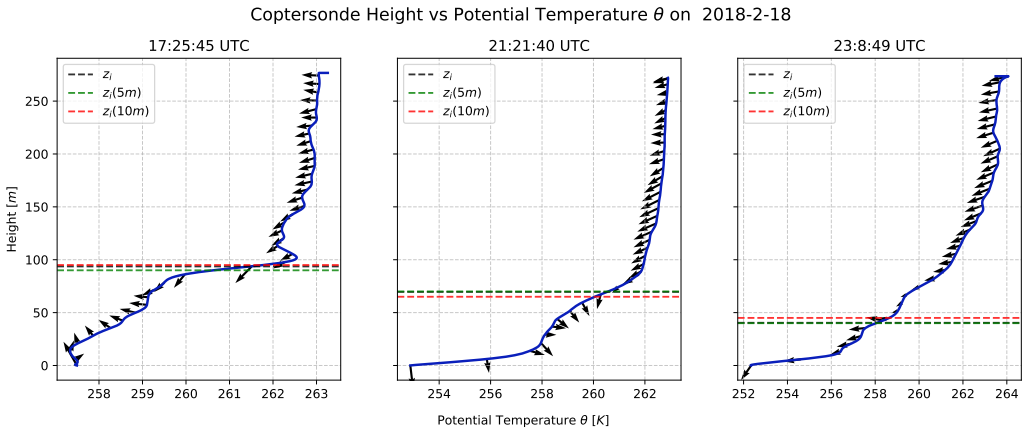

FIG. 3: CopterSonde potential temperature (K) profiles at three separate times during the night of February 18th, with horizontal wind vectors overlaid on top.

files the z_i heights occurs within the first 100 m from the surface, growing progressively lower with the later times in the second and third plots. This obvious decrease in height can be attributed to the shape of the temperature inversion evolving from a sharper inversion cap to a more subtle/non-existent capping as the night progresses. Observing more uniform temperature increases with height as in the later profiles introduces many challenges in defining one specific location where this gradient is maximum, and thus requires careful interpretation and further investigation before making decisions on that height's validity.

One of the first ways in investigating the validity of this z_i height is by looking at the data in differing vertical grid resolutions, as is done in Fig. 2b. Comparing z_i locations determined from gradients with different Δz helps to pinpoint erroneous maxima that can occur from any exceedingly small height differentials when calculating gradients. Looking at the z_i calculated from Δz of $<$1 m, 5 m, and 10 m respectively in Fig. 2b, no significant deviations appear with the altitudes, helping to verify that these locations of maximum temperature increase are not due to numerical errors and are more acceptable SBL heights. However, despite how consistently the gradient maximum occurs in the same location amidst differing data resolutions, the possibility of these z_i SBL heights being "false", or abnormally low, compared to other instances remains a major problem. The right-most plot in Fig. 2c demonstrates this phenomenon where filtering out any gradient maxima below 50 m altitude returns a much higher z_i ($\sim$75 m) than in that from Fig. 2b ($z_i \sim 50$ m). As past research studies have shown that SBLs can and have been found as low as 10 m-30 m (Banta et al. 2003), it is difficult to distinguish which z_i is the "correct" one, thus more detailed analysis of SBL characteristics is required to come to any immediate conclusions.

b. SBL depth determined by $\frac{\partial\theta}{\partial z}$ and u, v wind directions

To obtain a clearer understanding of why the temperature profiles behaved as they did on the night of February 18th, the $u(z)$ and $v(z)$ wind directions derived from the CopterSonde were introduced as a new criterion to better explain the turbulent motions occurring in the SBL and more accurately explain the locations of the SBL depths z_i. Fig. 3 shows the results of this in the form of wind vectors overlaid on the existing temperature profiles. Notice in each plot in Fig. 3 the overall direction of the horizontal winds differs below and above the z_i heights determined using potential temperatures. These added wind directions give a better picture of the SBL behavior during that particular night, and also help confirm the validity of the z_i locations determined via maximum gradients.

The behavior of the horizontal wind directions above and below the z_i is very interesting and introduces many questions as to the reason for that behavior around the SBL depth. For instance, why do the wind directions change below and above the SBL as defined by the z_i? Are the wind directions a consequence of the behavior of the temperature inversion, or is the converse true? Also, are the winds above the z_i due to the structure of the free atmosphere above the SBL, or are they the consequence of much larger-scale atmospheric motions such as cold-air advection? All of these questions and more present future opportunities for research into developing a new SBL depth parametrization integrating both potential temperature and wind directions.

c. SBL depth determined by $\frac{\partial\theta}{\partial z}$ and $|\mathbf{U}|$ maxima

The second, and final, SBL depth parametrization explored in this study was the altitude z_j where the horizontal windspeed $|\mathbf{U}|$ reaches a maximum, or the lowest height of the low level jet (LLJ) (Sullivan et al. 2016).

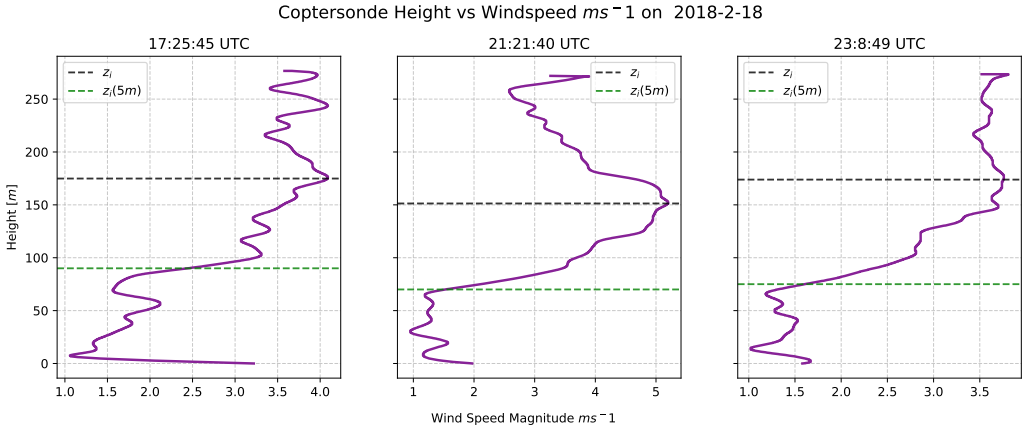

FIG. 4: CopterSonde wind speed (m s^{-1}) profiles at three separate times during the night of February 18th. Black dashed lines show the z_j height where maximum wind speeds are located, and the green dashed line shows the z_i height where the maximum potential temperature gradient is located.

Analyzing the $|\mathbf{U}|$ profiles taken from the CopterSonde, Fig. 4 displays the wind speed magnitudes as a function of height for the same three times as looked at in the previous figures. The black dashed lines in Fig. 4 show the height z_j where the maximum wind speeds were located, and are compared with the green dashed lines which represent the z_i heights previously calculated from the potential temperature gradients. Examining the z_i and z_j heights more carefully, it is immediately noticed that the z_j appears between 80 m-100 m above the z_i height. This observation prompts more questions such as the possible relationship, or lack thereof, between the maximum temperature gradient height z_i and the LLJ z_j, and its feasibility to be included as a parameter for defining a more precise SBL depth. With growing evidence of the coupling between LLJs and SBL characteristics such as TKE (Banta et al. 2007), the possibility of a coupling between z_i and z_j prompts this characteristic to be a possibility for future SBL depth parametrizations.

4. Conclusions

The premise of this study originally emerged from a need to improve our understanding of the stable boundary layer and increase the accuracy of existing climate models. The SBL depth in particular has long been a topic of much dispute and uncertainty, facing major discrepancies in definitions and parametrizations across literature and studies in recent years. Much of the variance in the SBL depth could be traced back to a larger-scale problem – a severe shortage of high-resolution observations of the SBL, and PBL in general. However, with the recent development of in-situ rwUAS systems, profiling the boundary layer on much higher spatial and temporal scales has become more practical and easily attainable than ever before. This study therefore aimed to take advantage of this new rwUAS technology with the University of Oklahoma's CopterSonde and attempt to use those higher-resolution observational profiles to create a new method of quantifying the stable boundary layer depth.

Observational data were examined from the 2018 Innovative Strategies for Observations in the Arctic Atmospheric Boundary Layer (ISOBAR) field campaign that took place in the Arctic region of northern Finland over sea ice. The observational datasets available from the CopterSonde included instantaneous temperature, horizontal wind speed, and wind direction profiles, therefore the most practical SBL depth definitions to examine with this data included the height z_i of the maximum potential temperature gradient and the height z_j of the maximum horizontal wind speeds. After comparing these SBL depths, several notable findings were recorded. The first was that many difficulties could arise locating a single temperature gradient maximum as high data resolutions could give falsely large gradients at low altitudes and the shape of the temperature inversions themselves could also create erroneously low SBL heights. The second finding was that analyzing the behaviors of the horizontal wind directions above and below the z_i heights could help determine the reasonableness of the calculated z_i height. The third finding was that the height z_j of the maximum wind speeds all occurred around 80 m-100 m above the z_i, implying that there could be a relationship between the two SBL characteristics.

These three findings point towards a much larger one, which is that all three variables – temperature, wind speed, and direction – are important in developing a better understanding of the SBL and where its depth may lie. In the larger picture, it may be difficult to pinpoint one exact altitude where the SBL ends and the free atmosphere begins

as the SBL depth is much more complex than discussed in this paper. However, obtaining a more in-depth picture of how different characteristics within the SBL behave and interact with each other can help to develop a much better understanding, and better parametrization, of the SBL in general.

The results of this case study also demonstrate the potential for applying rwUAS technology like the CopterSonde to more boundary layer problems. Due to previous limitations, the vast majority of SBL studies up until this point have focused on making conclusions from more traditional, and often lower-resolution, observational systems like radiosondes or Doppler lidars and sodars. Utilizing rwUAS to measure higher-resolution profiles can help to further validate, or disprove, the many turbulence and non-turbulence-based parametrizations currently being used to replicate aspects of the stable boundary layer. For example, a recent SBL study found the height of the maximum low-level jet h_j and the height h_1 of the first zero-crossing of wind shear profiles to be the most accurate estimates of the SBL depth based solely on lidar measurements (Pichugina and Banta 2010). Using rwUAS, a comparison study could be conducted to show the similarities and differences in SBL depth estimates using lidar data versus rwUAS data, and the results could reveal gaps in the measurements of either device and show where improvements can be made both in the instrumentation and existing boundary layer parameters. As this example shows, there is still a lot of work to be done in order to better understand and predict where the SBL depth may form on a given night. However, implementing rwUAS into solving these future research endeavors can help bring us one step closer to understanding the complexities of the stable boundary layer and predicting its depth.

Acknowledgments. This research has been supported by the National Science Foundation under Grant No. AGS-1560419. The authors would like to acknowledge the University of Oklahoma's Center for Autonomous Sensing and Sampling for their work in developing the CopterSonde, and all participants of the 2018 ISOBAR field campaign for providing the data to be used in this study. Also, much appreciation and thanks is extended to Dr. Daphne LaDue and Alex Marmo for coordinating and running a successful REU experience this summer despite working remotely. Finally, Theresa Lincheck would like to thank Brian Greene, Francesca Lappin, and Dr. Liz Pillar-Little for their amazing mentorship and support on this project during the course of this summer.

References

Banta, R. M., L. Mahrt, D. Vickers, J. Sun, B. B. Balsley, Y. L. Pichugina, and E. J. Williams, 2007: The Very Stable Boundary Layer on Nights with Weak Low-Level Jets. *Journal of the Atmospheric Sciences*, **64 (9)**, 3068–3090, doi:10.1175/JAS4002.1, URL https://doi.org/10.1175/JAS4002.1, https://journals.ametsoc.org/jas/article-pdf/64/9/3068/3497505/jas4002_1.pdf.

Banta, R. M., Y. L. Pichugina, and R. K. Newsom, 2003: Relationship between Low-Level Jet Properties and Turbulence Kinetic Energy in the Nocturnal Stable Boundary Layer. *Journal of the Atmospheric Sciences*, **60 (20)**, 2549–2555, doi:10.1175/1520-0469(2003)060⟨2549:RBLJPA⟩2.0.CO;2, URL https://doi.org/10.1175/1520-0469(2003)060⟨2549:RBLJPA⟩2.0.CO;2, https://journals.ametsoc.org/jas/article-pdf/60/20/2549/3468676/1520-0469(2003)060_2549_rbljpa_2_0_co_2.pdf.

Barbieri, L., and Coauthors, 2019: Intercomparison of Small Unmanned Aircraft System (sUAS) Measurements for Atmospheric Science during the LAPSE-RATE Campaign. *Sensors*, **19 (9)**, 2179, doi:10.3390/s19092179.

Beare, R. J., and Coauthors, 2006: An intercomparison of large-eddy simulations of the stable boundary layer. *Boundary-Layer Meteorology*, **118 (2)**, 247–272.

Bell, T. M., 2019: Confronting the boundary layer data gap: Evaluating new and existing methodologies of probing the lower atmosphere. *Boundary Layer, Urban Meteorology, and Land-Surface Processes Seminar Series*, University of Oklahoma School of Meteorology.

Bell, T. M., B. R. Greene, P. M. Klein, M. Carney, and P. B. Chilson, 2020: Confronting the boundary layer data gap: Evaluating new and existing methodologies of probing the lower atmosphere. *Atmospheric Measurement Techniques*, **13 (7)**, 3855–3872, doi:10.5194/amt-13-3855-2020.

Chilson, P. B., and Coauthors, 2019: Moving towards a Network of Autonomous UAS Atmospheric Profiling Stations for Observations in the Earth's Lower Atmosphere: The 3D Mesonet Concept. *Sensors*, **19 (12)**, 2720, doi:10.3390/s19122720.

Couvreux, F., and Coauthors, 2020: Intercomparison of Large-Eddy Simulations of the Antarctic Boundary Layer for Very Stable Stratification. *Boundary-Layer Meteorology*, doi:10.1007/s10546-020-00539-4.

Curry, J., 1983: On the Formation of Continental Polar Air. *Journal of the Atmospheric Sciences*, **40 (9)**, 2278–2292, doi:10.1175/1520-0469(1983)040⟨2278:OTFOCP⟩2.0.CO;2.

Greene, B. R., A. R. Segales, T. M. Bell, E. A. Pillar-Little, and P. B. Chilson, 2019: Environmental and Sensor Integration Influences on Temperature Measurements by Rotary-Wing Unmanned Aircraft Systems. *Sensors*, **19 (6)**, 1470, doi:10.3390/s19061470.

Greene, B. R., A. R. Segales, S. Waugh, S. Duthoit, and P. B. Chilson, 2018: Considerations for temperature sensor placement on rotary-wing unmanned aircraft systems. *Atmospheric Measurement Techniques*, **11 (10)**, 5519–5530, doi:10.5194/amt-11-5519-2018.

Hoff, R., and R. Hardesty, 2012: Thermodynamic Profiling Technologies Workshop Report to the National Science Foundation and the National Weather Service. Tech. rep., National Center for Atmospheric Research.

Huang, J., and E. Bou-Zeid, 2013: Turbulence and Vertical Fluxes in the Stable Atmospheric Boundary Layer. Part I: A Large-Eddy Simulation Study. *Journal of the Atmospheric Sciences*, **70 (6)**, 1513–1527, doi:10.1175/JAS-D-12-0167.1, URL https://doi.org/10.1175/JAS-D-12-0167.1, https://journals.ametsoc.org/jas/article-pdf/70/6/1513/3630575/jas-d-12-0167_1.pdf.

Kral, S., and Coauthors, 2020, in review: The innovative strategies for observations in the arctic atmospheric boundary layer project (ISOBAR). *Bull. Amer. Meteor. Soc.*

Kral, S. T., and Coauthors, 2018: Innovative strategies for observations in the arctic atmospheric boundary layer (ISOBAR)—the hailuoto 2017 campaign. *Atmosphere*, **9 (7)**, 268.

Mayfield, J. A., and G. J. Fochesatto, 2013: The Layered Structure of the Winter Atmospheric Boundary Layer in the Interior of Alaska. *Journal of Applied Meteorology and Climatology*, **52 (4)**, 953–973, doi:10.1175/JAMC-D-12-01.1, URL https://doi.org/10.1175/JAMC-D-12-01.1, https://journals.ametsoc.org/jamc/article-pdf/52/4/953/3570528/jamc-d-12-01_1.pdf.

National Academies of Sciences, E., 2018a: *The Future of Atmospheric Boundary Layer Observing, Understanding, and Modeling: Proceedings of a Workshop*. doi:10.17226/25138.

National Academies of Sciences, E., 2018b: *Thriving on Our Changing Planet: A Decadal Strategy for Earth Observation from Space*. doi:10.17226/24938.

National Research Council, 2007: *Earth Science and Applications from Space: National Imperatives for the Next Decade and Beyond*. National Academies Press.

Newman, J. F., and P. M. Klein, 2014: The Impacts of Atmospheric Stability on the Accuracy of Wind Speed Extrapolation Methods. *Resources*, **3 (1)**, 81–105, doi:10.3390/resources3010081.

Pichugina, Y. L., and R. M. Banta, 2010: Stable boundary layer depth from high-resolution measurements of the mean wind profile. *Journal of applied meteorology and climatology*, **49 (1)**, 20–35.

Pithan, F., B. Medeiros, and T. Mauritsen, 2014: Mixed-phase clouds cause climate model biases in Arctic wintertime temperature inversions. *Climate Dynamics*, **43 (1)**, 289–303, doi:10.1007/s00382-013-1964-9.

Sandu, I., A. Beljaars, P. Bechtold, T. Mauritsen, and G. Balsamo, 2013: Why is it so difficult to represent stably stratified conditions in numerical weather prediction (NWP) models? *Journal of Advances in Modeling Earth Systems*, **5 (2)**, 117–133, doi:10.1002/jame.20013.

Segales, A. R., B. R. Greene, T. M. Bell, W. Doyle, J. J. Martin, E. A. Pillar-Little, and P. B. Chilson, 2020: The coptersonde: an insight into the development of a smart unmanned aircraft system for atmospheric boundary layer research. *Atmospheric Measurement Techniques*, **13 (5)**.

Steeneveld, G. J., T. Mauritsen, E. I. F. de Bruijn, J. Vilà-Guerau de Arellano, G. Svensson, and A. a. M. Holtslag, 2008: Evaluation of Limited-Area Models for the Representation of the Diurnal Cycle and Contrasting Nights in CASES-99. *Journal of Applied Meteorology and Climatology*, **47 (3)**, 869–887, doi:10.1175/2007JAMC1702.1.

Stull, R. B., 1988: *An Introduction to Boundary Layer Meteorology*. 3rd ed., Kluwer Academic Publishers, 502-503 pp.

Sullivan, P. P., J. C. Weil, E. G. Patton, H. J. J. Jonker, and D. V. Mironov, 2016: Turbulent Winds and Temperature Fronts in Large-Eddy Simulations of the Stable Atmospheric Boundary Layer. *Journal of the Atmospheric Sciences*, **73 (4)**, 1815–1840, doi:10.1175/JAS-D-15-0339.1, URL https://doi.org/10.1175/JAS-D-15-0339.1, https://journals.ametsoc.org/jas/article-pdf/73/4/1815/4816016/jas-d-15-0339_1.pdf.